



Aalborg Universitet

AALBORG UNIVERSITY  
DENMARK

## Nonlinear periodic response analysis of mooring cables using harmonic balance method

Chen, Lin; Basu, Biswajit; Nielsen, Søren R.K.

*Published in:*  
Journal of Sound and Vibration

*DOI (link to publication from Publisher):*  
[10.1016/j.jsv.2018.09.027](https://doi.org/10.1016/j.jsv.2018.09.027)

*Creative Commons License*  
CC BY-NC-ND 4.0

*Publication date:*  
2019

*Document Version*  
Accepted author manuscript, peer reviewed version

[Link to publication from Aalborg University](#)

*Citation for published version (APA):*  
Chen, L., Basu, B., & Nielsen, S. R. K. (2019). Nonlinear periodic response analysis of mooring cables using harmonic balance method. *Journal of Sound and Vibration*, 438, 402-418.  
<https://doi.org/10.1016/j.jsv.2018.09.027>

### General rights

Copyright and moral rights for the publications made accessible in the public portal are retained by the authors and/or other copyright owners and it is a condition of accessing publications that users recognise and abide by the legal requirements associated with these rights.

- ? Users may download and print one copy of any publication from the public portal for the purpose of private study or research.
- ? You may not further distribute the material or use it for any profit-making activity or commercial gain
- ? You may freely distribute the URL identifying the publication in the public portal ?

### Take down policy

If you believe that this document breaches copyright please contact us at [vbn@aub.aau.dk](mailto:vbn@aub.aau.dk) providing details, and we will remove access to the work immediately and investigate your claim.

# Accepted Manuscript

Nonlinear periodic response analysis of mooring cables using harmonic balance method

Lin Chen, Biswajit Basu, Søren R.K. Nielsen



PII: S0022-460X(18)30612-6

DOI: [10.1016/j.jsv.2018.09.027](https://doi.org/10.1016/j.jsv.2018.09.027)

Reference: YJSVI 14378

To appear in: *Journal of Sound and Vibration*

Received Date: 22 November 2017

Revised Date: 11 July 2018

Accepted Date: 10 September 2018

Please cite this article as: L. Chen, B. Basu, Søren R.K. Nielsen, Nonlinear periodic response analysis of mooring cables using harmonic balance method, *Journal of Sound and Vibration* (2018), doi: <https://doi.org/10.1016/j.jsv.2018.09.027>.

This is a PDF file of an unedited manuscript that has been accepted for publication. As a service to our customers we are providing this early version of the manuscript. The manuscript will undergo copyediting, typesetting, and review of the resulting proof before it is published in its final form. Please note that during the production process errors may be discovered which could affect the content, and all legal disclaimers that apply to the journal pertain.

# Nonlinear periodic response analysis of mooring cables using harmonic balance method

Lin Chen<sup>a</sup>, Biswajit Basu<sup>a,\*</sup>, Søren R.K. Nielsen<sup>b</sup>

<sup>a</sup>*School of Engineering, Trinity College Dublin, Dublin 2, Ireland*

<sup>b</sup>*Department of Civil Engineering, Aalborg University, Aalborg 9000, Denmark*

## Abstract

Mooring cables are critical components of ocean renewable energy systems including offshore floating wind turbines and wave energy converters. Mooring cable dynamics is strongly nonlinear resulting from the geometric effect, hydrodynamic loads and probably seabed interactions. Time-domain methods are commonly used for numerical simulation. This study formulates a nonlinear frequency domain multi-harmonic balance method for efficient analysis of a mooring cable subjected to periodic fairlead motions. The periodic responses are of particular interest to investigate the mooring effect on the platform. In the formulation, the governing equations of the three-dimensional cable motions are spatially discretized using the finite difference method; the nonlinear ordinary differential equations are subsequently transformed into frequency domain by expanding both the structural responses and the nonlinear nodal forces using truncated Fourier series, leading to a set of nonlinear algebraic equations of the Fourier coefficients. The equations are eventually solved using Newton's method where the alternating frequency/time domain method is used to handle the nonlinearity effect. The presented method is then compared to a time-domain method by numerical studies of a mooring cable. The results show that the method is of comparable accuracy as the time-domain method while it is generally more efficient. The proposed method shows promising results even when the cable tension becomes non-positive for a period of time during the cable motion, which is a known ill-posed problem for time-domain methods.

**Keywords:** Mooring cables; nonlinear dynamics; harmonic balance method; periodic response; alternating frequency/time domain technique.

## 1. Introduction

Offshore winds and waves are promising renewable energy sources and are receiving intensive research attention recently. Modeling mooring systems is one of the challenging tasks in simulation and design of such floating offshore structures [1, 2]. Several comparison studies have already shown the importance of mooring cable dynamics on floating wind turbines [3–7]. In the last decade, a number of cable models have been explored, validated or coupled with the multi-body dynamics of floating offshore wind turbines and wave energy devices for numerical simulation, including the finite element model [8, 9], the multi-body dynamics model [10], the lumped mass models [11, 12] and the finite difference model [13–17]. A review of the available models and simulation tools of mooring cables can be found in [18, 19]. Presently, mathematical modeling of mooring cables is still a topic area, e.g. a high-order spectral method has been developed by [20, 21] and modeling cables using bar elements in an open-source library has been conducted in [22].

Despite a large number of models available for dynamic analyses of the mooring cables, the understanding of the mooring cable dynamics is still limited. This is due to the complex nonlinearity arising from the geometric effect, hydrodynamic loads and the seabed contact. Besides, for nonlinear analysis, hundreds of degrees of freedom of one

\*Corresponding author.

Email addresses: l.chen.tj@gmail.com (Lin Chen), basub@tcd.ie (Biswajit Basu), srkn@civil.aau.dk (Søren R.K. Nielsen)

## Nomenclature

$(\bar{\quad})$	variables are constant or dependent of cable static solution	$d$	cable diameter
$\mathbf{b}_{n-1/2}$	vectorized Fourier coefficients of $\hat{\mathbf{f}}_{n-1/2}$	$e$	error
$\mathbf{c}_k^{(\cdot)}, \mathbf{s}_k^{(\cdot)}$	Fourier coefficients of $\mathbf{y}_n$ or $\mathbf{f}_{n-1/2}$ , indicated by the superscripts	$EA$	cable axial stiffness
$\beta$	structural damping coefficient	$F_{dt}, F_{dn}, F_{db}$	drag forces per unit length in the local coordinate
$\mathbf{h}_{n-1/2}, \mathbf{h}_1, \mathbf{h}_N$	residual vector of the resulting nonlinear algebraic equations corresponding to intermediate and boundary nodes	$F_X, F_Y, F_Z$	fairlead forces
$\mathbf{I}_{(\quad)}$	identity matrix with dimension indicated by the subscript	$h, l$	static/initial cable depth and radius
$\mathbf{q}(t)$	vector containing the sine and cosine series	$i, j$	indexes
$\mathbf{y}(s, t) = [\tilde{\varepsilon} \ u \ v \ w \ \tilde{\phi} \ \tilde{\theta}]^T$	vector of nodal variables	$k$	index of harmonics in Fourier series
$\mathbf{z}_n$	vectorized Fourier coefficients of $\hat{\mathbf{y}}_n$	$L_0$	unstretched cable length
$\mathcal{F}^-, \mathcal{F}^+$	inverse FFT and FFT operators	$m$	cable mass per unit length
$\Delta \mathbf{z}_n$	increment of the Fourier coefficient vector	$m_a$	added mass per unit length
$(\dot{\quad})$	time derivatives	$N$	cable node number
$\Delta s_{n-1}$	cable segment length between node $n-1$ and node $n$	$n$	cable node index
$\gamma$	relaxation factor	$N_c$	number of Fourier coefficients for each unknown
$\hat{\mathbf{f}}_{n-1/2}$	vectorized $\tilde{\mathbf{f}}_{n-1/2}$ samples in one oscillation period	$N_h$	number of harmonics retained in truncated Fourier expansion
$\hat{\mathbf{y}}_n$	vectorized $\mathbf{y}_n$ samples in one oscillation period	$N_t$	number of time instances used for discretization the one period
$\mathbf{M}, \mathbf{K}, \mathbf{f}$	mass and stiffness matrices, and force vector after moving all nonlinear terms to the force vector	$N_y$	number of nodal variables
$\mathbf{Q}(\omega)$	Fourier series sampled at discrete time points	$s$	arc length coordinate of the unstretched cable
$\omega, T_f$	characteristic angular frequency and period of the forced fairlead motion	$t$	time
$\otimes$	Kronecker product operator	$u(s, t), v(s, t), w(s, t)$	cable velocity in tangential, normal and bi-normal directions in the moving Lagrangian reference frame
$\phi, \theta$	angles	$U(t), V(t), W(t)$	forced fairlead velocities at time $t$ and node $N$ in vertical, horizontal and out-of-plane directions of the fixed reference frame
$\rho_w$	the density of water	$U_c, V_c, W_c$	current velocities in the vertical and horizontal, and out-of-plane directions of the fixed reference coordinate system
$\Theta, \Theta_k$	partial differential operator in frequency domain and its block element	$u_r(s, t), v_r(s, t), w_r(s, t)$	relative velocities of the cable with respect to fluid current in the moving Lagrangian reference frame
$(\tilde{\quad})$	variables dependent of cable dynamic solution	$w_0$	submerged cable weight per unit length
$\nu$	an integer to account for subharmonics in Fourier series	$w_e$	effective cable submerged weight per unit length considering seabed effect
$\varepsilon(s, t)$	cable strain		
$C_{dt}, C_{dn}, C_{db}$	drag coefficients in tangential, normal and bi-normal directions of the moving Lagrangian coordinate system		

38 cable need to be considered for accuracy and hence the computational demand is another difficulty. Characterizing  
 39 the cable dynamics is important for improving the computational efficiency for the coupled analyses, e.g. by model  
 40 reduction and also for the interpretation of the coupled analysis results. In this context, this study focuses on the  
 41 research gap of nonlinear responses of a mooring cable subjected to periodic fairlead excitations, which represent an  
 42 important subset of the cable dynamics and also are important for understanding the nonlinear mooring loads on the  
 43 structures in the steady state. For understanding the dynamic behavior of submerged cables, linearization methods  
 44 [23–25] including linearization based frequency domain methods have been used to study towed cable dynamics [26].  
 45 The second-order nonlinear dynamics of catenary pipelines/cables have been studied using a perturbation technique

based on the finite difference model [27]. However, those methods can only give approximate solutions of the cable responses. In this study, the nonlinear periodic motion is proposed to be solved efficiently and accurately using a multi-Harmonic Balance (multi-HB) method.

The harmonic balance method may date back to [28–30] and it has been widely used as an efficient method for computing periodic and steady-state responses of nonlinear systems and, hence to gain insight into system nonlinear characteristics. Furthermore, the introduction of the Fast Fourier Transform (FFT) and the Alternating Frequency/Time (AFT) technique [31–34] enables the use of multiple (high-order) harmonics and accurate consideration of strong nonlinearity such as friction. With the AFT technique, it has been shown that the Jacobian matrix of the nonlinear algebraic equations resulting from multi-HB analysis can be formulated analytically, even for stiff systems with friction interfaces, which guarantees the computational efficiency. Currently, the multi-HB method is capable of studying the stability and nonlinear normal modes of large nonlinear systems as described in [35, 36]. It has been applied to aerospace structures [37], flexible structures with local nonlinear attachments [38–40], stay cables [41], and nonlinear mechanical systems [42], to name but a few. The single-term harmonic balance has been used for linearizing mooring dynamics by [24, 43, 44]. The multi-HB method, however, has not been applied to submerged cables with hydrodynamic effects so far.

This paper is structured as follows. After this introduction, Section 2 presents the nonlinear hydrodynamics of mooring cables along with a finite difference method for spatial discretization. Section 3 formulates the multi-HB method for mooring cables together with the AFT technique. Numerical studies are presented in Section 4 to demonstrate the effectiveness and advantages of the method by comparison with a time-domain method. A brief conclusion is provided in Section 5.

## 2. Nonlinear hydrodynamics of mooring cables

The mooring cable under consideration has uniform properties and circular or annular cross-section with the outer diameter  $d$ , mass per unit length  $m$ , and submerged weight per unit length  $w_0$  when unstretched. A linear strain and tension relationship is considered with  $EA$  denoting the axial stiffness. The unstretched cable length is denoted by  $L_0$ . The density of water is denoted by  $\rho_w$ . The initial cable depth and radius are denoted by  $h$  and  $l$  respectively, as shown in Fig. 1.

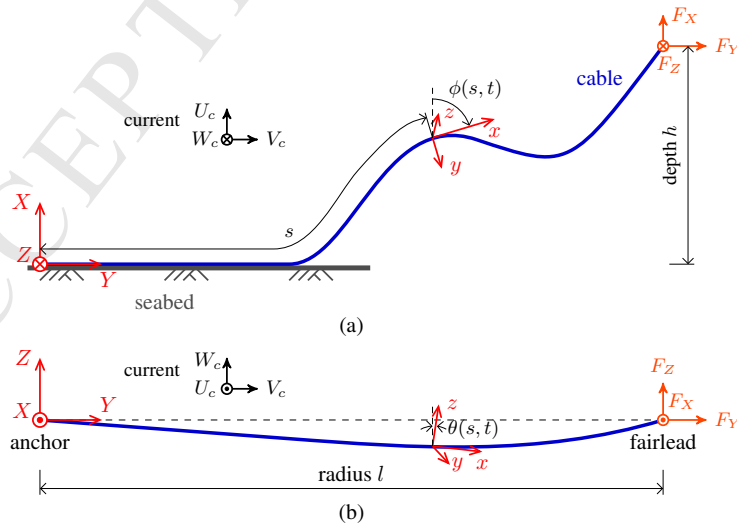


Figure 1: Submerged mooring cable and the coordinate system for describing its motion: (a) front view; (b) top view.

## 72 2.1. Governing Equations

73 The cable model derived in [13, 14] is used here. The bending and torsional stiffnesses are ignored because they  
 74 are quite small for mooring cables and hence have limited effects on the cable responses. The coordinate systems  
 75 for describing the three-dimensional mooring configuration and motion are shown in Fig. 1. The origin of the fixed  
 76 reference frame  $(X, Y, Z)$  is located at the cable anchorage on the seabed with  $X - Y$  plane as the vertical plane defined  
 77 by the anchor and the initial cable top end location and the  $X$ -axis is pointing upwards. A moving Lagrangian reference  
 78 frame  $(x, y, z)$  is attached to the cable at an arc length  $s$  of the unstretched cable measuring from the seabed anchor.  
 79 The  $x$ -axis is aligned with the local tangent direction. The angle between  $x$ -axis and  $X$ -axis in  $X - Y$  plane is denoted  
 80 by  $\phi$  and the angle between  $x$ -axis and  $Y$ -axis in  $Y - Z$  plane is denoted by  $\theta$ . The cable curvatures in the  $X - Y$  plane  
 81 and the  $Y - Z$  plane are then defined by  $\partial\phi/\partial s$  and  $\partial\theta/\partial s$  respectively. For the case concerned here where the cable is  
 82 axisymmetric and the bending and torsion are ignored, the two angles  $(\phi, \theta)$  along with  $s$  are found to be sufficient to  
 83 define the cable configuration [13]. The normal and binormal directions  $(y, z)$  of the local reference frame are defined  
 84 correspondingly after the transformation, using the two angles, to align  $X$ -axis to the local tangent direction.

85 Considering a steady current velocity with three components in the fixed reference frame, denoted by  $U_c$ ,  $V_c$  and  
 86  $W_c$  respectively, from the balance of forces in the Lagrangian reference frame together with the compatibility relations,  
 87 the partial differential equations (PDEs) governing the cable motion are given as [13]

$$0 = EA \frac{\partial \varepsilon}{\partial s} - m \frac{\partial u}{\partial t} + mv \cos \theta \frac{\partial \phi}{\partial t} - mw \frac{\partial \theta}{\partial t} + EA\beta \frac{\partial \varepsilon}{\partial t} - w_0 \cos \phi \cos \theta + F_{dt} \quad (1)$$

$$0 = EA\varepsilon \cos \theta \frac{\partial \phi}{\partial s} - (m + m_a) \frac{\partial v}{\partial t} - m(u \cos \theta + w \sin \theta) \frac{\partial \phi}{\partial t} - C_m \rho_w \frac{\pi d^2}{4} (U_c \cos \phi + V_c \sin \phi) \frac{\partial \phi}{\partial t} + w_0 \sin \phi + F_{dn} \quad (2)$$

$$0 = -EA\varepsilon \frac{\partial \theta}{\partial s} - (m + m_a) \frac{\partial w}{\partial t} + mv \sin \theta \frac{\partial \phi}{\partial t} - C_m \rho_w \frac{\pi d^2}{4} (U_c \sin \phi \sin \theta - V_c \cos \phi \sin \theta) \frac{\partial \phi}{\partial t} + mu \frac{\partial \theta}{\partial t} \\ + C_m \rho_w \frac{\pi d^2}{4} (U_c \cos \phi \cos \theta + V_c \sin \phi \cos \theta - W_c \sin \theta) \frac{\partial \theta}{\partial t} - w_0 \cos \phi \sin \theta + F_{db} \quad (3)$$

$$0 = \frac{\partial u}{\partial s} - \frac{\partial \varepsilon}{\partial t} + w \frac{\partial \theta}{\partial s} - v \frac{\partial \phi}{\partial s} \cos \theta \quad (4)$$

$$0 = \frac{\partial v}{\partial s} - (1 + \varepsilon) \cos \theta \frac{\partial \phi}{\partial t} + \frac{\partial \phi}{\partial s} \cos \theta (u + w \tan \theta) \quad (5)$$

$$0 = \frac{\partial w}{\partial s} + (1 + \varepsilon) \frac{\partial \theta}{\partial t} - v \frac{\partial \phi}{\partial s} \sin \theta - \frac{\partial \theta}{\partial s} u \quad (6)$$

88 where  $\varepsilon(s, t)$  = cable strain;  $u(s, t)$ ,  $v(s, t)$  and  $w(s, t)$  are the tangential, normal, and bi-normal components of cable  
 89 velocity. The buoyancy effect is included in calculation of the submerged weight per unit length  $w_0$ ; the Froude-  
 90 Krylov force, hydrodynamic mass and drag forces are considered using modified Morison's formula [45]. The added  
 91 mass is calculated by  $m_a = C_a \rho_w \pi d^2 / 4$  with the added mass coefficient denoted by  $C_a$ . The inertia coefficient is given  
 92 as  $C_m = 1 + C_a$ . A structural damping term is added into Eq. (1) as  $\beta EA \partial \varepsilon / \partial t$  assuming proportional damping [12].  
 93 The cable velocities relative to the fluid in the Lagrangian reference frame are denoted as  $u_r(s, t)$ ,  $v_r(s, t)$  and  $w_r(s, t)$ ,  
 94 i.e.

$$u_r = u - (U_c \cos \phi \cos \theta + V_c \sin \phi \cos \theta - W_c \sin \theta) \quad (7)$$

$$v_r = v - (-U_c \sin \phi + V_c \cos \phi) \quad (8)$$

$$w_r = w - (U_c \cos \phi \sin \theta + V_c \sin \phi \sin \theta + W_c \cos \theta) \quad (9)$$

95 The hydrodynamic drag forces are given as

$$F_{dt} = -\frac{1}{2}\rho_w d\pi C_{dt} |u_r| u_r \sqrt{1 + \varepsilon} \quad (10)$$

$$F_{dn} = -\frac{1}{2}\rho_w dC_{dn} v_r \sqrt{v_r^2 + w_r^2} \sqrt{1 + \varepsilon} \quad (11)$$

$$F_{db} = -\frac{1}{2}\rho_w dC_{db} w_r \sqrt{v_r^2 + w_r^2} \sqrt{1 + \varepsilon} \quad (12)$$

96 where  $C_{dt}$ ,  $C_{dn}$ , and  $C_{db}$  are the drag coefficients in tangential, normal and binormal directions.

## 97 2.2. Incremental form of the governing equations

98 For dynamic analysis, the static solution is assumed to be known, which fulfills the static equations that

$$0 = EA \frac{d\bar{\varepsilon}}{ds} - w_0 \cos \bar{\phi} \cos \bar{\theta} + \bar{F}_{dt} \quad (13)$$

$$0 = EA \bar{\varepsilon} \cos \bar{\theta} \frac{d\bar{\phi}}{ds} + w_0 \sin \bar{\phi} + \bar{F}_{dn} \quad (14)$$

$$0 = -EA \bar{\varepsilon} \frac{d\bar{\theta}}{ds} - w_0 \cos \bar{\phi} \sin \bar{\theta} + \bar{F}_{db} \quad (15)$$

99 where  $\bar{\varepsilon}$ ,  $\bar{\phi}$  and  $\bar{\theta}$  are the static solutions, and  $\bar{F}_{dt}$ ,  $\bar{F}_{dn}$  and  $\bar{F}_{db}$  are hydraulic drag forces when the cable is at rest. The  
100 preceding equations can be rewritten as

$$\frac{d\bar{\varepsilon}}{ds} = \frac{1}{EA} (w_0 \cos \bar{\phi} \cos \bar{\theta} - \bar{F}_{dt}) \quad (16)$$

$$\frac{d\bar{\phi}}{ds} = -\frac{1}{EA \bar{\varepsilon} \cos \bar{\theta}} (w_0 \sin \bar{\phi} + \bar{F}_{dn}) \quad (17)$$

$$\frac{d\bar{\theta}}{ds} = -\frac{1}{EA \bar{\varepsilon}} (w_0 \cos \bar{\phi} \sin \bar{\theta} - \bar{F}_{db}) \quad (18)$$

101 Correspondingly, the relative velocity of the static cable with respect to water is defined as

$$\bar{u}_r = -U_c \cos \bar{\phi} \cos \bar{\theta} - V_c \sin \bar{\phi} \cos \bar{\theta} + W_c \sin \bar{\theta}$$

$$\bar{v}_r = U_c \sin \bar{\phi} - V_c \cos \bar{\phi}$$

$$\bar{w}_r = -U_c \cos \bar{\phi} \sin \bar{\theta} - V_c \sin \bar{\phi} \sin \bar{\theta} - W_c \cos \bar{\theta}$$

102 The cable state can be expressed as the summation of its static and dynamic components as

$$\varepsilon(s, t) = \bar{\varepsilon}(s) + \tilde{\varepsilon}(s, t), \phi(s, t) = \bar{\phi}(s) + \tilde{\phi}(s, t), \theta(s, t) = \bar{\theta}(s) + \tilde{\theta}(s, t) \quad (19)$$

103 and hence the governing equations are rewritten in an incremental form as

$$0 = EA \frac{\partial(\bar{\varepsilon} + \tilde{\varepsilon})}{\partial s} - m \frac{\partial u}{\partial t} + mv \cos \theta \frac{\partial \tilde{\phi}}{\partial t} - mw \frac{\partial \tilde{\theta}}{\partial t} + EA\beta \frac{\partial \tilde{\varepsilon}}{\partial t} - w_0 \cos \phi \cos \theta + F_{dt} \quad (20)$$

$$0 = EA(\bar{\varepsilon} + \tilde{\varepsilon}) \cos \theta \frac{\partial(\bar{\phi} + \tilde{\phi})}{\partial s} - (m + m_a) \frac{\partial v}{\partial t} - m [u \cos \theta + w \sin \theta] \frac{\partial \tilde{\phi}}{\partial t} - C_m \rho_w \frac{\pi d^2}{4} (U_c \cos \phi + V_c \sin \phi) \frac{\partial \tilde{\phi}}{\partial t} + w_0 \sin \phi + F_{dn} \quad (21)$$

$$0 = -EA\varepsilon \frac{\partial(\bar{\theta} + \tilde{\theta})}{\partial s} - (m + m_a) \frac{\partial w}{\partial t} + mv \sin \theta \frac{\partial \tilde{\phi}}{\partial t} - C_m \rho_w \frac{\pi d^2}{4} (U_c \sin \phi \sin \theta - V_c \cos \phi \sin \theta) \frac{\partial \tilde{\phi}}{\partial t} + mu \frac{\partial \tilde{\theta}}{\partial t} + C_m \rho_w \frac{\pi d^2}{4} (U_c \cos \phi \cos \theta + V_c \sin \phi \cos \theta - W_c \sin \theta) \frac{\partial \tilde{\theta}}{\partial t} - w_0 \cos \phi \sin \theta + F_{db} \quad (22)$$

$$0 = \frac{\partial u}{\partial s} - \frac{\partial \tilde{\varepsilon}}{\partial t} + w \frac{\partial(\bar{\theta} + \tilde{\theta})}{\partial s} - v \frac{\partial(\bar{\phi} + \tilde{\phi})}{\partial s} \cos(\bar{\theta} + \tilde{\theta}) \quad (23)$$

$$0 = \frac{\partial v}{\partial s} - (1 + \bar{\varepsilon} + \tilde{\varepsilon}) \cos(\theta + \tilde{\theta}) \frac{\partial \tilde{\phi}}{\partial t} + \frac{\partial(\bar{\phi} + \tilde{\phi})}{\partial s} \cos(\bar{\theta} + \tilde{\theta}) [u + w \tan(\bar{\theta} + \tilde{\theta})] \quad (24)$$

$$0 = \frac{\partial w}{\partial s} + (1 + \bar{\varepsilon} + \tilde{\varepsilon}) \frac{\partial \tilde{\theta}}{\partial t} - v \frac{\partial(\bar{\phi} + \tilde{\phi})}{\partial s} \sin(\bar{\theta} + \tilde{\theta}) - \frac{\partial(\bar{\theta} + \tilde{\theta})}{\partial s} u \quad (25)$$

### 104 2.3. Equations in matrix form

105 The PDEs using the incremental formulation can be written in matrix form as

$$\mathbf{M}(\mathbf{y}) \frac{\partial \mathbf{y}}{\partial t} + \mathbf{K}(\mathbf{y}) \frac{\partial \mathbf{y}}{\partial s} + \mathbf{f}(\mathbf{y}) = 0 \quad (26)$$

106 where the nodal state vector is  $\mathbf{y}(s, t) = [\tilde{\varepsilon}, u, v, w, \tilde{\phi}, \tilde{\theta}]^T$ ,  $\mathbf{M}$  and  $\mathbf{K}$  are mass and stiffness matrices, and  $\mathbf{f}$  is the nodal  
107 force vector. They are given as below

$$\mathbf{K} = \begin{bmatrix} EA & 0 & 0 & 0 & 0 & 0 \\ 0 & 0 & 0 & 0 & EA\varepsilon \cos \theta & 0 \\ 0 & 0 & 0 & 0 & 0 & -EA\varepsilon \\ 0 & 1 & 0 & 0 & -v \cos \theta & w \\ 0 & 0 & 1 & 0 & u \cos \theta + w \sin \theta & 0 \\ 0 & 0 & 0 & 1 & -v \sin \theta & -u \end{bmatrix} \quad (27)$$

$$\mathbf{M} = \begin{bmatrix} EA\beta & -m & 0 & 0 & mv \cos \theta & -mw \\ 0 & 0 & -(m + m_a) & 0 & M_{2,5} & 0 \\ 0 & 0 & 0 & -(m + m_a) & M_{3,5} & M_{3,6} \\ -1 & 0 & 0 & 0 & 0 & 0 \\ 0 & 0 & 0 & 0 & M_{5,5} & 0 \\ 0 & 0 & 0 & 0 & 0 & 1 + \varepsilon \end{bmatrix} \quad (28)$$

109 where

$$M_{2,5} = -m(w \sin \theta + u \cos \theta) - C_m \rho_w \frac{\pi d^2}{4} (U_c \cos \phi + V_c \sin \phi)$$

$$M_{3,5} = mv \sin \theta - C_m \rho_w \frac{\pi d^2}{4} (U_c \sin \phi \sin \theta - V_c \cos \phi \sin \theta)$$

$$M_{3,6} = mu + C_m \rho_w \frac{\pi d^2}{4} (U_c \cos \phi \cos \theta + V_c \sin \phi \cos \theta - W_c \sin \theta)$$

$$M_{5,5} = -(1 + \varepsilon) \cos \theta$$



110 and the force vector  $\mathbf{f} = [f_1 \ f_2 \ f_3 \ f_4 \ f_5 \ f_6]^T$

$$f_1 = -w_0 \cos \phi \cos \theta + F_{dt} + EA \frac{d\bar{\varepsilon}}{ds} \quad (29)$$

$$f_2 = w_0 \sin \phi + F_{dn} - EA\varepsilon \cos \theta \frac{d\bar{\phi}}{ds} \quad (30)$$

$$f_3 = -w_0 \cos \phi \sin \theta + F_{db} - EA\varepsilon \frac{d\bar{\theta}}{ds} \quad (31)$$

$$f_4 = -v \cos \theta \frac{d\bar{\phi}}{ds} + w \frac{d\bar{\theta}}{ds} \quad (32)$$

$$f_5 = (u \cos \theta + w \sin \theta) \frac{d\bar{\phi}}{ds} \quad (33)$$

$$f_6 = -v \sin \theta \frac{d\bar{\phi}}{ds} + u \frac{d\bar{\theta}}{ds} \quad (34)$$

111 Noting that  $\mathbf{M}$ ,  $\mathbf{K}$  and  $\mathbf{f}$  depend on  $\mathbf{y}$ , for the convenience of formulating the harmonic balance analysis, the  
112 governing equations are rewritten by collecting all the  $\mathbf{y}$ -dependent terms in the nodal force vector such that

$$\bar{\mathbf{M}} \frac{\partial \mathbf{y}}{\partial t} + \bar{\mathbf{K}} \frac{\partial \mathbf{y}}{\partial s} + \tilde{\mathbf{M}}(\mathbf{y}) \frac{\partial \mathbf{y}}{\partial t} + \tilde{\mathbf{K}}(\mathbf{y}) \frac{\partial \mathbf{y}}{\partial s} + \mathbf{f}(\mathbf{y}) = \mathbf{0} \quad (35)$$

113 The mass and stiffness matrices, and force vector thus become

$$\bar{\mathbf{M}} = \begin{bmatrix} EA\beta & -m & 0 & 0 & 0 & 0 \\ 0 & 0 & -m - m_a & 0 & 0 & 0 \\ 0 & 0 & 0 & -m - m_a & 0 & 0 \\ -1 & 0 & 0 & 0 & 0 & 0 \\ 0 & 0 & 0 & 0 & -(1 + \bar{\varepsilon}) \cos \bar{\theta} & 0 \\ 0 & 0 & 0 & 0 & 0 & 1 + \bar{\varepsilon} \end{bmatrix} \quad (36)$$

$$\bar{\mathbf{K}} = \begin{bmatrix} EA & 0 & 0 & 0 & 0 & 0 \\ 0 & 0 & 0 & 0 & EA\bar{\varepsilon} \cos \bar{\theta} & 0 \\ 0 & 0 & 0 & 0 & 0 & -EA\bar{\varepsilon} \\ 0 & 1 & 0 & 0 & 0 & 0 \\ 0 & 0 & 1 & 0 & 0 & 0 \\ 0 & 0 & 0 & 1 & 0 & 0 \end{bmatrix} \quad (37)$$

115 and

$$\tilde{\mathbf{M}} = \begin{bmatrix} 0 & 0 & 0 & 0 & mv \cos \theta & -mw \\ 0 & 0 & 0 & 0 & M_{2,5} & 0 \\ 0 & 0 & 0 & 0 & M_{3,5} & M_{3,6} \\ 0 & 0 & 0 & 0 & 0 & 0 \\ 0 & 0 & 0 & 0 & M_{5,5} + (1 + \bar{\varepsilon}) \cos \bar{\theta} & 0 \\ 0 & 0 & 0 & 0 & 0 & \bar{\varepsilon} \end{bmatrix}, \quad \tilde{\mathbf{K}} = \begin{bmatrix} 0 & 0 & 0 & 0 & 0 & 0 \\ 0 & 0 & 0 & 0 & EA\varepsilon \cos \theta - EA\bar{\varepsilon} \cos \bar{\theta} & 0 \\ 0 & 0 & 0 & 0 & 0 & -EA\bar{\varepsilon} \\ 0 & 0 & 0 & 0 & -v \cos \theta & w \\ 0 & 0 & 0 & 0 & u \cos \theta + w \sin \theta & 0 \\ 0 & 0 & 0 & 0 & -v \sin \theta & -u \end{bmatrix} \quad (38)$$

116 As in [13–16], Eq. (26) along with boundary conditions can be discretized in both time and space using the finite  
117 difference method and then solved using the relaxation method [46]. For formulating the multi-HB analysis, the  
118 equation is only spatially discretized using the finite difference method.

#### 119 2.4. Spatial discretization

120 For spatial discretization, the spatial derivatives Eq. (26) are replaced by the central differences [13, 16]. Let the  
121 cable be discretized into  $N - 1$  segments with  $N$  nodal points in total along the cable length. The first node is at the

122 seabed origin and the  $N$ th node is at the cable top end. Hence, a set of  $N - 1$  matrix equations (one equation per half  
123 grid) can be obtained as

$$\begin{aligned} [\bar{\mathbf{M}}_{n-1} \quad \bar{\mathbf{M}}_n] \begin{Bmatrix} \dot{\mathbf{y}}_{n-1} \\ \dot{\mathbf{y}}_n \end{Bmatrix} + \frac{1}{\Delta s_{n-1}} [-\bar{\mathbf{K}}_{n-1} - \bar{\mathbf{K}}_n \quad \bar{\mathbf{K}}_{n-1} + \bar{\mathbf{K}}_n] \begin{Bmatrix} \mathbf{y}_{n-1} \\ \mathbf{y}_n \end{Bmatrix} + [\tilde{\mathbf{M}}_{n-1} \quad \tilde{\mathbf{M}}_n] \begin{Bmatrix} \dot{\mathbf{y}}_{n-1} \\ \dot{\mathbf{y}}_n \end{Bmatrix} \\ + \frac{1}{\Delta s_{n-1}} [-\tilde{\mathbf{K}}_{n-1} - \tilde{\mathbf{K}}_n \quad \tilde{\mathbf{K}}_{n-1} + \tilde{\mathbf{K}}_n] \begin{Bmatrix} \mathbf{y}_{n-1} \\ \mathbf{y}_n \end{Bmatrix} + \mathbf{f}_{n-1} + \mathbf{f}_n = \mathbf{0} \end{aligned} \quad (39)$$

124 which is further written as

$$[\bar{\mathbf{M}}_{n-1} \quad \bar{\mathbf{M}}_n] \begin{Bmatrix} \dot{\mathbf{y}}_{n-1} \\ \dot{\mathbf{y}}_n \end{Bmatrix} + [-\bar{\mathbf{K}}_{n-1/2} \quad \bar{\mathbf{K}}_{n-1/2}] \begin{Bmatrix} \mathbf{y}_{n-1} \\ \mathbf{y}_n \end{Bmatrix} + \tilde{\mathbf{f}}_{n-1/2} = \mathbf{0} \quad (40)$$

125 with

$$\begin{aligned} \bar{\mathbf{K}}_{n-1/2} &= (\bar{\mathbf{K}}_{n-1} + \bar{\mathbf{K}}_n) / \Delta s_{n-1}, \\ \tilde{\mathbf{f}}_{n-1/2} &= [\tilde{\mathbf{M}}_{n-1} \quad \tilde{\mathbf{M}}_n] \begin{Bmatrix} \dot{\mathbf{y}}_{n-1} \\ \dot{\mathbf{y}}_n \end{Bmatrix} + \frac{1}{\Delta s_{n-1}} [-\tilde{\mathbf{K}}_{n-1} - \tilde{\mathbf{K}}_n \quad \tilde{\mathbf{K}}_{n-1} + \tilde{\mathbf{K}}_n] \begin{Bmatrix} \mathbf{y}_{n-1} \\ \mathbf{y}_n \end{Bmatrix} + \mathbf{f}_{n-1} + \mathbf{f}_n \end{aligned} \quad (41)$$

## 126 2.5. Boundary conditions

127 The cable is often fixed at the seabed anchor such that the velocity at the first node is constantly zero

$$u_1 = 0, v_1 = 0, w_1 = 0 \quad (42)$$

128 On the other hand, the fairlead is subjected to excitations resulting from platform motion. Let the excitation velocity  
129 be represented by its three components in the fixed cable coordinate system, i.e.  $U(t)$ ,  $V(t)$  and  $W(t)$  respectively.  
130 Hence, the boundary equations at the fairlead node are given at time  $t$  as

$$0 = u_N \cos \phi_N \cos \theta_N - v_N \sin \phi_N + w_N \cos \phi_N \sin \theta_N - U(t) \quad (43)$$

$$0 = u_N \sin \phi_N \cos \theta_N + v_N \cos \phi_N + w_N \sin \phi_N \sin \theta_N - V(t) \quad (44)$$

$$0 = -u_N \sin \theta_N + w_N \cos \theta_N - W(t) \quad (45)$$

131 Correspondingly the cable tension at the fairlead has three components in the fixed cable coordinate system, as illus-  
132 trated in Fig. 1, given as

$$F_X(t) = EA \varepsilon_N \cos \phi_N \cos \theta_N \quad (46)$$

$$F_Y(t) = EA \varepsilon_N \sin \phi_N \cos \theta_N \quad (47)$$

$$F_Z(t) = -EA \varepsilon_N \sin \theta_N \quad (48)$$

133 In cases where the fairlead force is known, the preceding three equations are the boundary conditions at the fairlead.  
134 This is usually the case for static analysis.

135 The mooring cable usually lies partly grounded on the seabed to avoid the lift force to the anchor. For considering  
136 the cable-seabed contact effect, the method proposed in [15] is adopted herein. Flat seabed is considered and it is  
137 modeled as elastic spring with stiffness  $k_{sb}$  which provides a vertical support force when the cable is grounded. This  
138 can be easily accounted for by modifying the effective submerged cable weight. In other words, the effective weight  
139 per unit length at node  $n$  is given as  $w_e^n = w_0 + k_{sb} X(s_n)$  and  $0 \leq w_e^n \leq w_0$  for static problem. In solving the PDEs using  
140 iterative method, to consider the seabed effect,  $w_0$  in Eqs. (29-34) is replaced by  $w_e^n$  which is evaluated based on the  
141 cable nodal position obtained in the previous iteration step. After solving the equations in the Lagrangian coordinate  
142 system, the cable nodal displacement and position can be integrated node by node from the seabed anchor using  $s$ ,  $\phi$   
143 and  $\theta$  [13, 15].

### 144 3. Multi-harmonic balance analysis

145 The nonlinear ordinary equation (39) can also be solved in time domain by replacing the time derivatives using  
 146 finite differences [16]. However, the time domain method may be subjected to numerical stability issues and to obtain  
 147 the steady-state responses and a long time simulation may be required to arrive the steady state. This section therefore  
 148 formulates the multi-HB method for efficiently solving the cable responses when it is subjected to periodic fairlead  
 149 excitations.

#### 150 3.1. Governing equations in frequency domain

151 Considering the cable subjected to a periodic excitation with a period  $T_f$  and the corresponding characteristic  
 152 angular frequency  $\omega = 2\pi/T_f$  at its fairlead, the periodic cable response  $\mathbf{y}_n$  is pursued herein and hence the nodal  
 153 force  $\mathbf{f}_n$  is also periodic. Therefore, they can be approximated using truncated Fourier series as follows,

$$154 \mathbf{y}_n(t) \approx \frac{\mathbf{c}_0^{y_n}}{\sqrt{2}} + \sum_{k=1}^{N_h} \left( \mathbf{s}_k^{y_n} \sin \frac{k\omega t}{\nu} + \mathbf{c}_k^{y_n} \cos \frac{k\omega t}{\nu} \right) \quad (49)$$

$$155 \tilde{\mathbf{f}}_{n-1/2}(t) \approx \frac{\mathbf{c}_0^{f_{n-1/2}}}{\sqrt{2}} + \sum_{k=1}^{N_h} \left( \mathbf{s}_k^{f_{n-1/2}} \sin \frac{k\omega t}{\nu} + \mathbf{c}_k^{f_{n-1/2}} \cos \frac{k\omega t}{\nu} \right) \quad (50)$$

156 in which the index  $k$  represents the  $k$ th harmonic component and  $N_h =$  the number of harmonics retained. Noting  
 157 that generally the constant terms need to be retained since the presence of the current may induce constant drift of the  
 158 solution. The total number of coefficient for each degree of freedom is denoted by  $N_c = 2N_h + 1$  for general cases and  
 159  $N_c = 2N_h$  if the constant term is omitted. The integer  $\nu$  accounts for subharmonics of the excitation frequency  $\omega$ . The  
 coefficients  $\mathbf{c}_k^{(\cdot)}$  and  $\mathbf{s}_k^{(\cdot)}$  can be reshaped to  $N_c N_y \times 1$  vectors as

$$160 \mathbf{z}_n = \left[ c_0^{y_{n,1}} \ s_1^{y_{n,1}} \ c_1^{y_{n,1}} \ \dots \ s_{N_h}^{y_{n,1}} \ c_{N_h}^{y_{n,1}} \ \dots \ s_{N_h}^{y_{n,N_y}} \ c_{N_h}^{y_{n,N_y}} \right]^T \quad (51)$$

$$161 \mathbf{b}_{n-1/2} = \left[ c_0^{f_{n-1/2,1}} \ s_1^{f_{n-1/2,1}} \ c_1^{f_{n-1/2,1}} \ \dots \ s_{N_h}^{f_{n-1/2,1}} \ c_{N_h}^{f_{n-1/2,1}} \ \dots \ s_{N_h}^{f_{n-1/2,N_y}} \ c_{N_h}^{f_{n-1/2,N_y}} \right]^T \quad (52)$$

162 where  $N_y$  denotes the number of variables at each node, i.e.  $N_y = 6$  here. Note that the coefficient arrangements here  
 163 are different from [47] for the convenience of using relaxation method in the subsequent solving procedure [46]. Then  
 the nodal response and force can be recast into a compact form as

$$164 \mathbf{y}_n(t) = \left[ \mathbf{I}_{N_y} \otimes \mathbf{q}(t) \right] \mathbf{z}_n \quad (53)$$

$$165 \mathbf{f}_{n-1/2}(t) = \left[ \mathbf{I}_{N_y} \otimes \mathbf{q}(t) \right] \mathbf{b}_{n-1/2} \quad (54)$$

166 where  $\otimes$  stands for an operation on two matrices which gives another matrix that is formed by multiplying the second  
 167 matrix by each element of the first matrix (known as Kronecker product of two matrices, see Appendix A for an  
 example). The matrix  $\mathbf{I}_{N_y}$  is an identity matrix of size  $N_y \times N_y$ , and  $\mathbf{q}(t)$  is a row vector containing the sine and cosine  
 series

$$168 \mathbf{q}(t) = \left[ \frac{1}{\sqrt{2}} \ \sin \frac{\omega t}{\nu} \ \cos \frac{\omega t}{\nu} \ \dots \ \sin \frac{k\omega t}{\nu} \ \cos \frac{k\omega t}{\nu} \ \dots \ \sin \frac{N_h \omega t}{\nu} \ \cos \frac{N_h \omega t}{\nu} \right] \quad (55)$$

From Eq. (53), one obtains

$$169 \dot{\mathbf{y}}_n(t) = \left[ \mathbf{I}_{N_y} \otimes \mathbf{q}(t) \right] \dot{\mathbf{z}}_n = \left\{ \mathbf{I}_{N_y} \otimes [\mathbf{q}(t)\Theta] \right\} \dot{\mathbf{z}}_n \quad (56)$$

in which the matrix  $\Theta$  is given as

$$170 \Theta = \begin{bmatrix} \Theta_1 & & & & \\ & \ddots & & & \\ & & \Theta_k & & \\ & & & \ddots & \\ & & & & \Theta_{N_h} \end{bmatrix} \quad (57)$$

170 with block entries that

$$\Theta_k = \begin{bmatrix} 0 & -k\omega/\nu \\ k\omega/\nu & 0 \end{bmatrix} \quad (58)$$

171 Substituting expressions (53,56) into Eq. (39), one obtains

$$[\bar{\mathbf{M}}_{n-1} \ \bar{\mathbf{M}}_n] \{ \mathbf{I}_{N_y} \otimes [\mathbf{q}(t)\Theta] \} \begin{Bmatrix} \mathbf{z}_{n-1} \\ \mathbf{z}_n \end{Bmatrix} + [-\bar{\mathbf{K}}_{n-1/2} \ \bar{\mathbf{K}}_{n-1/2}] \mathbf{I}_{N_y} \otimes \mathbf{q}(t) \begin{Bmatrix} \mathbf{z}_{n-1} \\ \mathbf{z}_n \end{Bmatrix} + [\mathbf{I}_{N_y} \otimes \mathbf{q}(t)] \mathbf{b}_{n-1/2} = \mathbf{0}_{N_y \times 1} \quad (59)$$

172 where  $\mathbf{0}_{N_y \times 1}$  represents a vector of size  $N_y$  containing zeros. The preceding equation can be further simplified as

$$\{ [\bar{\mathbf{M}}_{n-1} \ \bar{\mathbf{M}}_n] \otimes [\mathbf{q}(t)\Theta] \} \begin{Bmatrix} \mathbf{z}_{n-1} \\ \mathbf{z}_n \end{Bmatrix} + \{ [-\bar{\mathbf{K}}_{n-1/2} \ \bar{\mathbf{K}}_{n-1/2}] \otimes \mathbf{q}(t) \} \begin{Bmatrix} \mathbf{z}_{n-1} \\ \mathbf{z}_n \end{Bmatrix} + [\mathbf{I}_{N_y} \otimes \mathbf{q}(t)] \mathbf{b}_{n-1/2} = \mathbf{0}_{N_y \times 1} \quad (60)$$

173 To eliminate the time dependency of the preceding equation, a Galerkin procedure projects the preceding equation  
174 on the orthogonal trigonometric basis of  $\mathbf{q}(t)$ , namely

$$\begin{aligned} \left\{ [\bar{\mathbf{M}}_{n-1} \ \bar{\mathbf{M}}_n] \otimes \left[ \frac{2}{T_f} \int_0^{T_f} \mathbf{q}^\top(t)\mathbf{q}(t)dt \Theta \right] + [-\bar{\mathbf{K}}_{n-1/2} \ \bar{\mathbf{K}}_{n-1/2}] \otimes \left[ \frac{2}{T_f} \int_0^{T_f} \mathbf{q}^\top(t)\mathbf{q}(t)dt \right] \right\} \begin{Bmatrix} \mathbf{z}_{n-1} \\ \mathbf{z}_n \end{Bmatrix} \\ + \left\{ \mathbf{I}_{N_y} \otimes \left[ \frac{2}{T_f} \int_0^{T_f} \mathbf{q}^\top(t)\mathbf{q}(t)dt \right] \right\} \mathbf{b}_{n-1/2} = \mathbf{0}_{N_y \times 1} \end{aligned} \quad (61)$$

175 Note that

$$\frac{2}{T_f} \int_0^{T_f} \mathbf{q}^\top(t)\mathbf{q}(t)dt = \mathbf{I}_{N_c}$$

176 The governing equations are eventually expressed in frequency domain as

$$\{ [\bar{\mathbf{M}}_{n-1} \ \bar{\mathbf{M}}_n] \otimes \Theta + [-\bar{\mathbf{K}}_{n-1/2} \ \bar{\mathbf{K}}_{n-1/2}] \otimes \mathbf{I}_{N_c} \} \begin{Bmatrix} \mathbf{z}_{n-1} \\ \mathbf{z}_n \end{Bmatrix} + \mathbf{b}_{n-1/2} = \mathbf{0}_{N_c N_y \times 1} \quad (62)$$

177 The the left-hand side of the preceding equation is defined as the residual, i.e.

$$\mathbf{h}_{n-1/2} = [\bar{\mathbf{M}}_{n-1} \otimes \Theta - \bar{\mathbf{K}}_{n-1/2} \otimes \mathbf{I}_{N_c} \ \bar{\mathbf{M}}_n \otimes \Theta + \bar{\mathbf{K}}_{n-1/2} \otimes \mathbf{I}_{N_c}] \begin{Bmatrix} \mathbf{z}_{n-1} \\ \mathbf{z}_n \end{Bmatrix} + \mathbf{b}_{n-1/2} \quad (63)$$

178 for each intermediate node  $1 < n \leq N$ . Similarly, for the boundary nodes, it reads

$$\mathbf{h}_1 = \mathbf{b}_1, \quad \mathbf{h}_N = \mathbf{b}_N \quad (64)$$

179 For implementation of multi-HB method, it is crucial to determine  $\mathbf{b}_n$  and also the Jacobian matrix for gradient based  
180 correction of the solution. The AFT method is applied [32], as detailed in the following subsection.

### 181 3.2. AFT technique for handling nonlinearity

182 The expressions for the nonlinear nodal forces as expressed in Eq. (29-34) are difficult to be analytically trans-  
183 formed into frequency domain to obtain the coefficients in the Fourier series. The AFT technique offers a convenient  
184 procedure as

$$\mathbf{z}_n, \mathbf{z}_{n-1} \xrightarrow{\mathcal{F}^-} \mathbf{y}_n, \mathbf{y}_{n-1}, \dot{\mathbf{y}}_n, \dot{\mathbf{y}}_{n-1} \rightarrow \tilde{\mathbf{f}}_{n-1/2} \xrightarrow{\mathcal{F}^+} \mathbf{b}_{n-1/2} \quad (65)$$

185 where  $\mathcal{F}^-$  denotes the inverse FFT operator and correspondingly the FFT operator is denoted by  $\mathcal{F}^+$ . In other words,  
186 in each iteration step, the nonlinear nodal force is obtained by evaluating Eq. (29-34) in time domain, using time  
187 series of the nodal state which are transformed from  $\mathbf{z}_n$  and  $\mathbf{z}_{n-1}$  using inverse FFT, and further the nodal force time  
188 series are transformed into frequency domain for  $\mathbf{b}_n$  and  $\mathbf{b}_{n-1}$  via FFT.

189 Let the time period be discretized by  $N_t$  equally distributed sampling points in the FFT. One can define vectors  $\hat{\mathbf{y}}$   
 190 and  $\hat{\mathbf{f}}$  containing the concatenated  $N_t \cdot N_y$  time samples of the nodal states and the forces, respectively. For the  $n$ th  
 191 node, one thus obtains

$$\hat{\mathbf{y}}_n = [y_{n,1}(t_1) \cdots y_{n,1}(t_{N_t}) \cdots y_{n,N_y}(t_1) \cdots y_{n,N_y}(t_{N_t})]^\top \quad (66)$$

$$\hat{\mathbf{f}}_{n-1/2} = [\tilde{f}_{n-1/2,1}(t_1) \cdots \tilde{f}_{n-1/2,1}(t_{N_t}) \cdots \tilde{f}_{n-1/2,N_y}(t_1) \cdots \tilde{f}_{n-1/2,N_y}(t_{N_t})]^\top \quad (67)$$

192 The inverse FFT can then be written as a linear operation

$$\hat{\mathbf{y}}_n = \mathcal{F}^- \mathbf{z}_n, \hat{\mathbf{f}}_{n-1/2} = \mathcal{F}^- \mathbf{b}_{n-1/2} \quad (68)$$

193 with the sparse operator

$$\mathcal{F}^- = \mathbf{I}_{N_y} \otimes \mathbf{Q}(\omega) \quad (69)$$

194 where  $\mathbf{Q}(\omega)$  is the matrix of the time samples of trigonometrical functions

$$\mathbf{Q}(\omega) = \begin{bmatrix} \frac{1}{\sqrt{2}} & \sin \frac{\omega t_1}{v} & \cos \frac{\omega t_1}{v} & \cdots & \sin \frac{N_h \omega t_1}{v} & \cos \frac{N_h \omega t_1}{v} \\ \frac{1}{\sqrt{2}} & \sin \frac{\omega t_2}{v} & \cos \frac{\omega t_2}{v} & \cdots & \sin \frac{N_h \omega t_2}{v} & \cos \frac{N_h \omega t_2}{v} \\ \vdots & \vdots & \vdots & \ddots & \vdots & \vdots \\ \frac{1}{\sqrt{2}} & \sin \frac{\omega t_{N_t}}{v} & \cos \frac{\omega t_{N_t}}{v} & \cdots & \sin \frac{N_h \omega t_{N_t}}{v} & \cos \frac{N_h \omega t_{N_t}}{v} \end{bmatrix} \quad (70)$$

195 Similarly, the FFT to obtain the Fourier coefficients is written as

$$\mathbf{z}_n = \mathcal{F}^+ \hat{\mathbf{y}}_n, \mathbf{b}_{n-1/2} = \mathcal{F}^+ \hat{\mathbf{f}}_{n-1/2} \quad (71)$$

196 where the FFT operator is computed by  $\mathcal{F}^+ = (\mathcal{F}^-)^\top [(\mathcal{F}^-)^\top]^{-1}$ .

197 The Jacobian matrix of the residual function (63) with respect to  $\mathbf{z}_{n-1}$  and  $\mathbf{z}_n$  can be obtained as

$$\frac{\partial \mathbf{h}_{n-1/2}}{\partial \mathbf{z}_{n-1}} = (\bar{\mathbf{M}}_{n-1} \otimes \boldsymbol{\Theta} - \bar{\mathbf{K}}_{n-1/2} \otimes \mathbf{I}_{N_c}) + \frac{\partial \mathbf{b}_{n-1/2}}{\partial \mathbf{z}_{n-1}} \quad (72)$$

$$\frac{\partial \mathbf{h}_{n-1/2}}{\partial \mathbf{z}_n} = (\bar{\mathbf{M}}_n \otimes \boldsymbol{\Theta} + \bar{\mathbf{K}}_{n-1/2} \otimes \mathbf{I}_{N_c}) + \frac{\partial \mathbf{b}_{n-1/2}}{\partial \mathbf{z}_n} \quad (73)$$

199 The difficulty in evaluating the Jacobian matrix lies in the computation of  $\partial \mathbf{b}_{n-1/2} / \partial \mathbf{z}_n$ . This also requires the AFT  
 200 technique. Noting that  $\hat{\mathbf{f}}_{n-1/2}$  is a function of both  $\mathbf{y}_n$  and  $\dot{\mathbf{y}}_n$  so that the Jacobian matrix computation needs to be  
 201 written as

$$\begin{aligned} \frac{\partial \mathbf{b}_{n-1/2}}{\partial \mathbf{z}_n} &= \frac{\partial \mathbf{b}_{n-1/2}}{\partial \hat{\mathbf{f}}_{n-1/2}} \frac{\partial \hat{\mathbf{f}}_{n-1/2}}{\partial \mathbf{z}_n} = \mathcal{F}^+ \frac{\partial \hat{\mathbf{f}}_{n-1/2}}{\partial \mathbf{z}_n} \\ &= \mathcal{F}^+ \left( \frac{\partial \hat{\mathbf{f}}_{n-1/2}}{\partial \dot{\mathbf{y}}_n} \frac{\partial \dot{\mathbf{y}}_n}{\partial \mathbf{z}_n} + \frac{\partial \hat{\mathbf{f}}_{n-1/2}}{\partial \mathbf{y}_n} \frac{\partial \mathbf{y}_n}{\partial \mathbf{z}_n} \right) = \mathcal{F}^+ \frac{\partial \hat{\mathbf{f}}_{n-1/2}}{\partial \dot{\mathbf{y}}_n} \mathcal{F}^- + \mathcal{F}^+ \frac{\partial \hat{\mathbf{f}}_{n-1/2}}{\partial \mathbf{y}_n} \{ \mathbf{I}_{N_y} \otimes [\mathbf{Q}(\omega) \boldsymbol{\Theta}] \} \end{aligned} \quad (74)$$

202 Similar procedure is applicable for computing  $\partial \mathbf{b}_{n-1/2} / \partial \mathbf{z}_{n-1}$ . The same method is also applied for handling the  
 203 boundary nodal equations (64) but it is noteworthy that the FFT operator for boundary equations is of size  $N_c \times 3N_t$   
 204 here. From Eqs. (29-34)  $\partial \hat{\mathbf{f}}_{n-1/2} / \partial \mathbf{y}_n$  and  $\partial \hat{\mathbf{f}}_{n-1/2} / \partial \dot{\mathbf{y}}_n$  can be derived analytically (see Appendix B), which are then  
 205 evaluated at the sampled time instances in a period and further rearranged to obtain  $\partial \hat{\mathbf{f}}_{n-1/2} / \partial \mathbf{y}_n$  and  $\partial \hat{\mathbf{f}}_{n-1/2} / \partial \dot{\mathbf{y}}_n$ .  
 206 Once the residual and Jacobian matrix are available, Newton's method can be used for iteration to solve the equation.  
 207 In addition, for this two-point boundary valued problem spatially discretized using the first-order finite difference,  
 208 only the two neighboring nodes are coupled and hence the problem can be solved from the fairlead node by node  
 209 without assembling the global mass, stiffness matrices and the force vector. In iteration for solving the equations, the  
 210 coefficient vector  $\mathbf{z}_n$  for all the nodes are updated by

$$\mathbf{z}_n^{i+1} = \mathbf{z}_n^i + \gamma \Delta \mathbf{z}_n^i \quad (75)$$

211 where  $\Delta \mathbf{z}_n^i$  is the state increment,  $\gamma$  is the relaxation factor which is in the range of 0 and 1 to slow the update, and  $i$  is  
 212 the iteration step index. The adjustment method of the relaxation factor proposed in [16] is applied here.

213 The error is defined as [16]

$$e^i = \frac{1}{N_c N} \sum_{n=1}^N \sum_{j=1}^{N_c} |\Delta z_{n,j}^i| \quad (76)$$

### 214 3.3. Solving procedure

215 Providing the cable and environmental parameters and the cable static solution, the presented method can be used  
 216 to conduct periodic responses analysis. Given the forced motion frequency, the FFT and inverse FFT operators can be  
 217 prepared for use. The solving procedure is summarized as below.

- 218 i Evaluate  $\tilde{\mathbf{M}}_n$  and  $\tilde{\mathbf{K}}_n$  for  $1 \leq n \leq N$  from the static solution using Eqs. (36,37);
- 219 ii Initialize  $\mathbf{z}_n$  for all nodes;
- 220 iii Evaluate  $\hat{\mathbf{y}}_n$  and  $\dot{\hat{\mathbf{y}}}_n$  using the inverse FFT, Eq. (68), and rearrange the vector to obtain  $\mathbf{y}_n(t_j)$  and  $\dot{\mathbf{y}}_n(t_j)$  for all  
 221 nodes and time instances;
- 222 iv Evaluate  $\tilde{\mathbf{M}}_n$ ,  $\tilde{\mathbf{K}}_n$  and  $\tilde{\mathbf{f}}_n$  for all nodes using Eqs. (38,29–34);
- 223 v Evaluate  $\tilde{\mathbf{f}}_{n-1/2}$ ,  $\partial \tilde{\mathbf{f}}_{n-1/2} / \partial \mathbf{y}_n$ ,  $\partial \tilde{\mathbf{f}}_{n-1/2} / \partial \mathbf{y}_{n-1}$ ,  $\tilde{\mathbf{f}}_{n-1/2} / \partial \dot{\mathbf{y}}_n$  and  $\tilde{\mathbf{f}}_{n-1/2} / \partial \dot{\mathbf{y}}_{n-1}$  using Eq. (40) and for boundary nodes  
 224 using Eqs. (42-45);
- 225 vi Rearrange  $\tilde{\mathbf{f}}_{n-1/2}$  for all nodes and time instances to obtain  $\hat{\mathbf{f}}_{n-1/2}$  and rearrange  $\tilde{\mathbf{f}}_{n-1/2} / \partial \mathbf{y}_n$  and  $\tilde{\mathbf{f}}_{n-1/2} / \partial \mathbf{y}_{n-1}$  to  
 226 obtain  $\hat{\mathbf{f}}_{n-1/2} / \partial \hat{\mathbf{y}}_n$ ,  $\hat{\mathbf{f}}_{n-1/2} / \partial \hat{\mathbf{y}}_{n-1}$ ,  $\hat{\mathbf{f}}_{n-1/2} / \partial \dot{\hat{\mathbf{y}}}_{n-1}$  and  $\hat{\mathbf{f}}_{n-1/2} / \partial \dot{\hat{\mathbf{y}}}_{n-1}$ ;
- 227 vii Obtain  $\mathbf{h}_{n-1/2}$  using Eq. (63) and  $\mathbf{h}_1$  and  $\mathbf{h}_N$  using Eq. (64) and  $\partial \mathbf{h}_{n-1/2} / \partial \mathbf{z}_n$  and  $\partial \mathbf{h}_{n-1/2} / \partial \mathbf{z}_n$  using Eqs. (72,73)  
 228 with the FFT and inverse FFT operators;
- 229 viii Solve  $\Delta \mathbf{z}_n$  and evaluate the error and update  $\mathbf{z}_n$  using Eq. (75);
- 230 ix Check the error using Eq. (76) and repeat steps 3-8 before convergence.
- 231 x Stop if convergence is achieved or the maximum number of iterations is reached.

232 The method is implemented in C++ with Eigen library [48] for handling linear algebra, matrix and vector operations.

## 233 4. Application and discussion

234 In this section, a typical mooring cable is analyzed using the presented method and the results are compared with  
 235 corresponding time-domain analysis results. The open-source mooring system simulation program developed by the  
 236 authors, named OpenMOOR, which has been verified and applied in [7, 49], is used for the time-domain analysis.  
 237 The generalized- $\alpha$  method is used for time stepping [50].

### 238 4.1. Description of the simulated mooring cable

239 The mooring cable of the OC3 Hywind platform for the spar-type floating offshore wind turbine is used [51, 52].  
 240 The cable properties are listed in Table 1 along with the hydrodynamic coefficients which are adopted following [5].  
 241 In the following numerical analyses, to focus on the multi-HB method, the cable is considered to be in still water and  
 242 the seabed interaction is ignored here. In this case, the constant terms in the Fourier expansion, i.e. Eqs. (49,50), are  
 243 omitted. Hence  $N_c = 2N_h$  and correspondingly the first column of the matrix  $\mathbf{Q}(\omega)$  in Eq. (70) is also eliminated.

244 The cable static profile is shown in Fig. 2 which is solved using a shooting procedure [15]. The cable is divided  
 245 into 49 segments with 50 nodes. For a fair comparison of the computation efficiency, in using the time-domain method,  
 246 the static solution is used as the starting point. In harmonic balance analysis, the static solution is used along with  
 247 zero dynamic responses as initial guess, i.e.  $\mathbf{z}_n = \mathbf{0}$ .

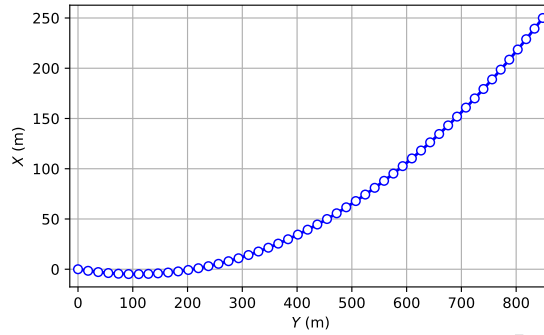


Figure 2: Static profile of the simulated cable (circles indicate the node position).

Table 1: Cable properties and environmental parameters

Parameter	Symbol	Unit	Value
Diameter	$d$	m	0.09
Unstretched length	$L_0$	m	902.2
Mass per unit length	$m$	kg/m	77.7066
Submerged weight per unit length	$w_0$	N/m	698.094
Elastic stiffness	$EA$	N	3.84243E8
Static cable depth	$h$	m	250
Static cable radius	$l$	m	848.67
Added mass coefficient	$C_a$	-	1.0
Drag coefficient	$C_{dt}, C_{dn}, C_{db}$	-	0, 1.6, 1.6

#### 248 4.2. Convergence of the multi-HB method

249 The convergence of the presented method is first studied. The cable is forced with harmonic motions at the  
 250 fairlead in the  $Y$  direction (surge motion). The frequency is considered to be 0.05 Hz when the non-linearity effect  
 251 can be clearly seen in the following results. In using the multi-HB method, the integer  $\nu = 1$  is adopted since no sub-  
 252 harmonic responses have been observed in this case; the initial relaxation factor is set to be 1.0, and the convergence  
 253 tolerance is considered to be  $10^{-10}$ . The first case considers the amplitude of the fairlead displacement to be 5.0 m and  
 254 in a second case, the amplitude is increased to 9.0 m. The error evolution with respect to the iteration step is plotted in  
 255 Fig. 3 and the obtained cable tensions,  $EA\varepsilon$ , at the fairlead are plotted in Fig. 4. Results solved using different values  
 256 of the harmonic balance parameters are presented for comparison.

257 It can be seen from Fig. 3 that for all the cases, the computation is able to achieve a fast convergence within  
 258 ten steps. Generally, more iterations are required when higher-order harmonics are included and a larger number of  
 259 time points are used. More importantly, even for the difficult case when cable tension becomes non-positive during  
 260 the cable motion, which is known as an ill-posed problem for perfectly flexible cables [53], convergence can still  
 261 be achieved with the multi-HB method, as shown in Fig. 4 for the case when the forced motion has an amplitude  
 262 of 9.0 m and the fairlead tension is zero around  $t = 15$  s. This is because the Jacobian matrix of the multi-HB  
 263 method is constructed from all the time instances in one period and therefore it is nonsingular even if the Jacobian  
 264 matrix of the time-domain equation is singular for some time instances. In Fig. 4, by comparing the results obtained  
 265 using 9 harmonics and more, it can be concluded that the solution is converged with 9 harmonics in these two cases.  
 266 Actually, with 3 harmonics the method can already achieve a quite high accuracy as compared to those obtained using  
 267 9 harmonics.

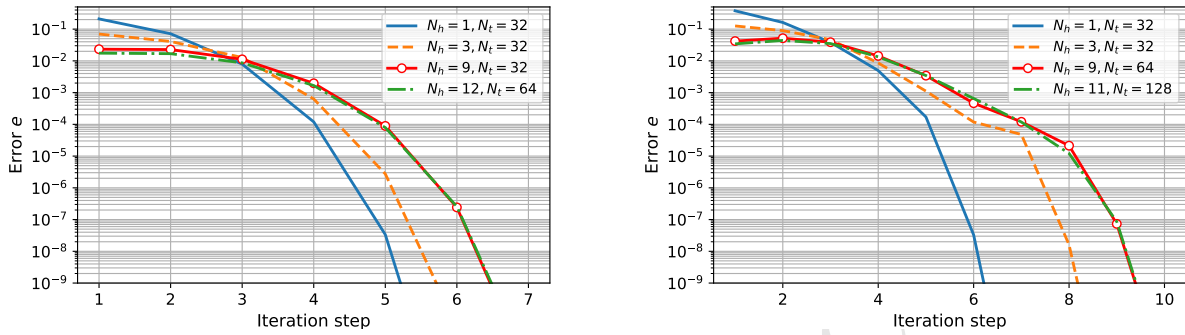


Figure 3: Error evolution in the multi-HB analysis (left) forced fairlead motion in  $Y$  direction of amplitude 5.0 m; (right) forced fairlead motion in  $Y$  direction of amplitude 9.0 m.

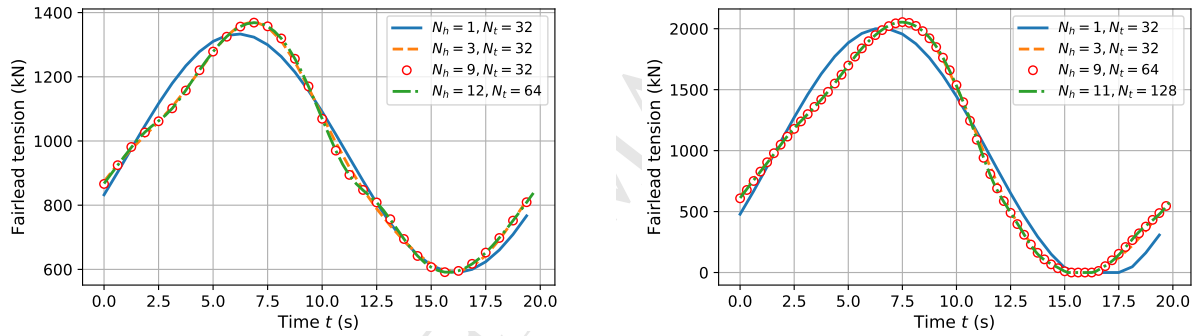


Figure 4: Fairlead tensions solved using the multi-HB method (left) forced fairlead motion in  $Y$  direction of amplitude 5.0 m; (right) forced fairlead motion in  $Y$  direction of amplitude 9.0 m.

#### 268 4.3. Comparison of time- and frequency-domain methods

269 To verify the presented method and to show its advantages, simulations are carried out with the comparison to  
 270 the time-domain method. As shown in the preceding section,  $N_h = 9$  and  $N_t = 32$  are sufficient for the convergence  
 271 of the multi-HB analysis and they are thus adopted in the following analysis. In using the time-domain method, the  
 272 convergence tolerance is also set to be  $10^{-10}$ . Time domain analyses commonly start with the static solution with  
 273 zero displacements and zero velocity, and hence some time is required to dissipate the transient responses so that  
 274 the cable motion can reach the steady state. In the analysis, the displacement is ramped to the target value in half  
 275 of a period and therefore at least two periods are required. The time needed for the transient responses to dying out  
 276 depends on the system damping. For mooring cables, due to the hydrodynamic drag effect, several periods may be  
 277 sufficient. As shown in Fig. 5, with the transverse drag coefficient of 1.6 in Table 1, the solution reaches the steady  
 278 state in 3 periods, while decreasing the drag coefficient to 0.1, at least four periods are required. The accuracy and  
 279 computational efficiency also depend on the time step, a test shows that a time step of 0.1 s is the minimum step to  
 280 prevent the numerical drift of the cable displacement at the fairlead which is a known issue of this finite difference  
 281 cable modal [16]. In the following, the time step is considered to be 0.1 s and the time-domain analysis is performed  
 282 for three periods of the forced motion. The cable responses in the third period are assumed to be the steady responses  
 283 to be compared with the harmonic balance analysis results.

284 Four cases are studied for comparison. In the first three cases, a forced motion of a displacement amplitude of 5.0  
 285 m and frequency of 0.05 Hz is considered respectively in  $Y$ ,  $X$ , and  $Z$  directions. In the last case, the forced motion  
 286 is considered in both  $Y$  and  $Z$  directions: the motion in the  $Y$  direction has a displacement amplitude of 2.5 m and



287 frequency of 0.1 Hz and the motion in the  $Z$  direction is of a displacement amplitude of 5.0 m and a frequency of  
 288 0.05 Hz. The computation times to obtain the steady-state response using the time-domain method and the multi-HB  
 289 method are compared in Table 2. Note that the value listed for the time-domain method is the time taken to complete  
 290 a three-period simulation. The computations were performed on a 16-core Windows desktop (Intel i7-8700 CPU @  
 291 3.20 GHz). It is seen that the multi-HB method is much efficient and the computational time is almost equivalent to  
 292 the time needed to run the time-domain method for one period. Additionally, for such a nonlinear system, the time  
 293 required for the system to reach the steady state is not known beforehand and for systems with less damping, more  
 294 time is required as shown in Fig. 5.

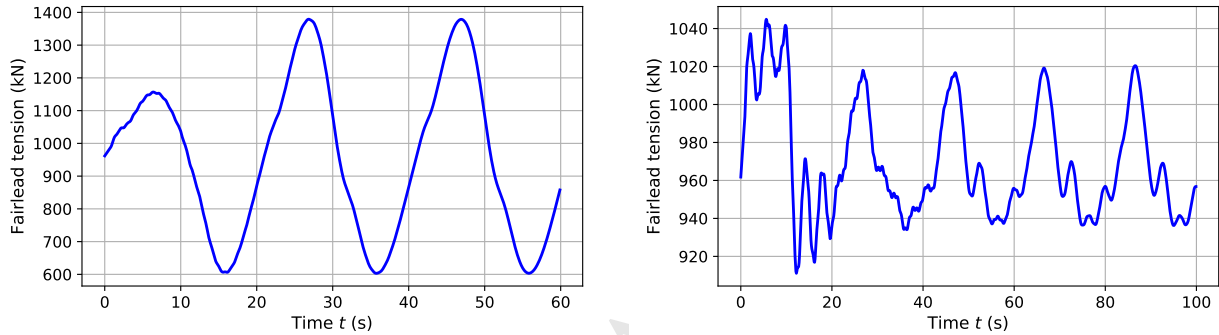


Figure 5: Fairlead tension time history solved using the time domain method (left) with hydrodynamic drag coefficients  $C_{dt} = 0$  and  $C_{dn} = C_{db} = 1.6$ ; (right) with hydrodynamic drag coefficients  $C_{dt} = 0$  and  $C_{dn} = C_{db} = 0.1$ .

Table 2: Computational efficiency comparison

Case no.	Time-domain computation (s)	Multi-HB computation (s)	Description
1	6.03	1.40	motion in $Y$ direction
2	6.07	1.40	motion in $X$ direction
3	6.47	2.43	motion in $Z$ direction
4	6.74	3.01	motion in both $Y$ and $Z$ direction

295 The cable responses solved using the time-domain method and the multi-HB are compared in Figs. 6–9 where the  
 296 fairlead tension and the nodal solution corresponding to the 25th node (with  $s = 441.11$  m) are plotted. In most of the  
 297 graphics, results obtained using the two methods are found to be pretty consistent. Relatively observable differences  
 298 are seen in the fairlead tension and the nodal strain of Fig. 8 when the forced motion is in the out-of-plane direction.  
 299 This is because the overall tension/strain variation is small since the forced motion is in the out-of-plane. Besides, the  
 300 super-harmonic responses are clearly captured in the cable tension, as also reported in the numerical study using time  
 301 domain methods by [54].

302 The numerical results clearly demonstrate that in the analyzed cases, the multi-HB method has achieved compa-  
 303 rable accuracy as the time-domain analysis while it is more efficient. In addition, as seen from the solving procedure  
 304 given in Section 3.3, the AFT technique requires the FFT and inverse FFT operations for all nodes which can be done  
 305 in parallel for further improving the computational efficiency. To summarize, the multi-HB method is found to be  
 306 advantageous for periodic analyses of mooring cables.

## 307 5. Conclusion

308 This study has proposed and formulated a multi-HB method for a three-dimensional mooring cable under periodic  
 309 fairlead motion. The governing equations of the cable are first represented in an incremental form and then spatially  
 310 discretized using the finite difference method. The nodal equations are transformed into the frequency domain by

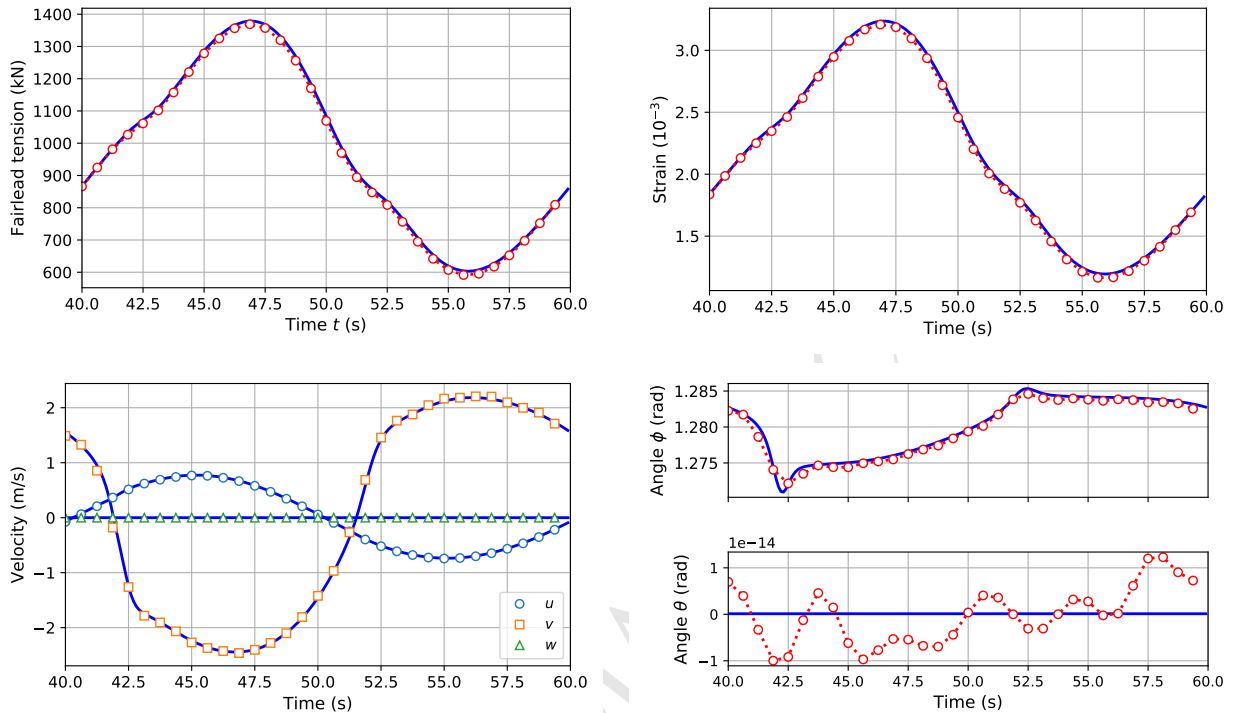


Figure 6: Comparison of the fairlead tension and nodal solution corresponding to the 25th node with  $s = 441.11$  m when the forced motion is in  $Y$  direction. Lines correspond to the time-domain analysis results and symbols indicate the multi-HB analysis results.

311 Fourier expansion. The AFT technique is applied to handle the geometrical and hydrodynamic non-linearity accu-  
 312 rately. The presented method is implemented and compared with a time domain method based on numerical studies  
 313 of a typical mooring cable. The following conclusions can be drawn:

- 314 i The multi-HB method together with the AFT technique is promising to solve periodic mooring cable motion. It  
 315 can handle the geometric and hydrodynamic nonlinearity and the case when cable tension becomes zero.
- 316 ii The multi-HB method is accurate and more efficient as compared to the time-domain method for analyzing the  
 317 periodic cable responses.
- 318 iii The method is able to capture the super-harmonic cable responses and is promising for further parametric analyses  
 319 of mooring cables.

320 Future studies will focus on local and global stability analysis of mooring cables with nonlinear hydrodynamics based  
 321 on the presented method.

## 322 Acknowledgments

323 This work was partly supported by the Irish Research Council (IRC) via the Government of Ireland Postdoctoral  
 324 Fellowship (Project ID: GOIPD/2017/1260) and the European Unions Horizon 2020 research and innovation pro-  
 325 gramme under the Marie Skłodowska-Curie EID project ICONN Grant Agreement No. 675659, which is gratefully  
 326 acknowledged.

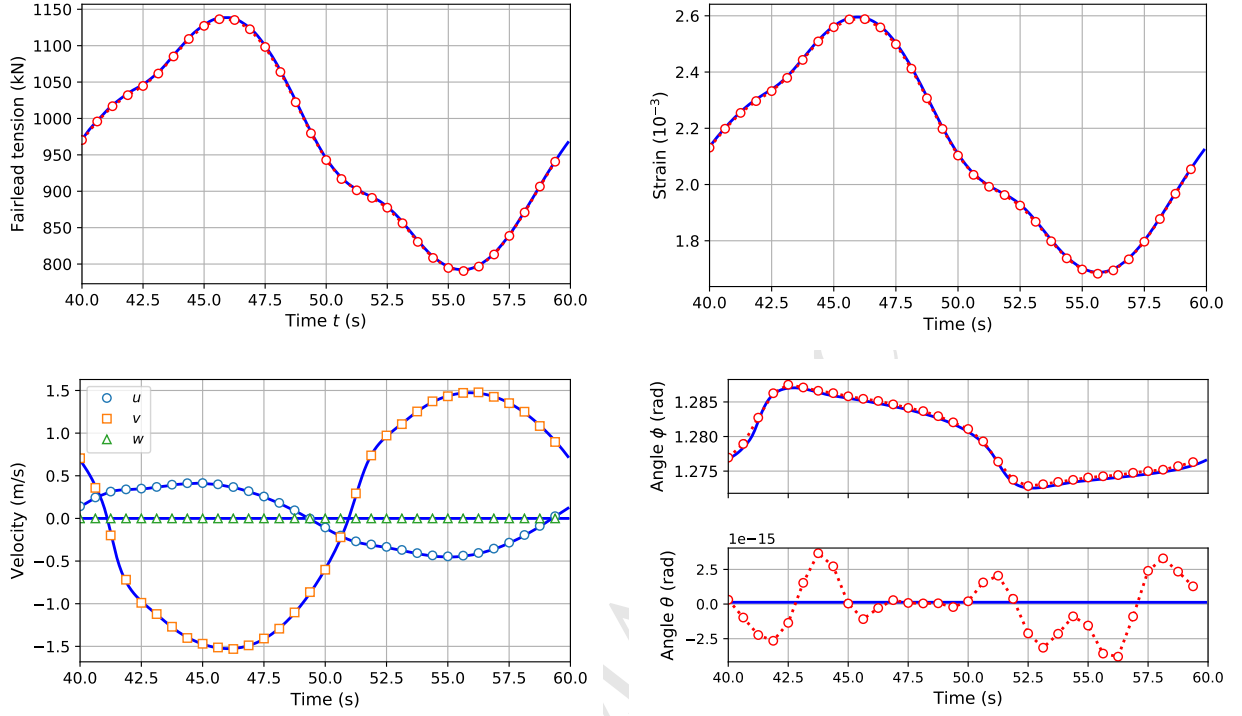


Figure 7: Comparison of the fairlead tension and nodal solution corresponding to the 25th node with  $s = 441.11$  m when the forced motion is in  $X$  direction. Lines correspond to the time-domain analysis results and symbols indicate the multi-HB analysis results.

### 327 Appendix A. Kronecker product

The Kronecker product of two matrices is calculated by

$$\mathbf{A} \otimes \mathbf{E} = \begin{bmatrix} a_{11} & a_{12} & \cdots & a_{1q} \\ a_{21} & a_{22} & \cdots & a_{2q} \\ \vdots & \vdots & \ddots & \vdots \\ a_{p1} & a_{p2} & \cdots & a_{pq} \end{bmatrix} \otimes \mathbf{E} = \begin{bmatrix} a_{11}\mathbf{E} & a_{12}\mathbf{E} & \cdots & a_{1q}\mathbf{E} \\ a_{21}\mathbf{E} & a_{22}\mathbf{E} & \cdots & a_{2q}\mathbf{E} \\ \vdots & \vdots & \ddots & \vdots \\ a_{p1}\mathbf{E} & a_{p2}\mathbf{E} & \cdots & a_{pq}\mathbf{E} \end{bmatrix}$$

328 where  $a_{(.,.)} \in \mathbb{R}$  is an element of matrix  $\mathbf{A}$  ( $p \times q$ ).

### 329 Appendix B. Matrix differentiation

330 In the derivation of  $\partial \tilde{\mathbf{f}}_{n-1/2} / \partial \mathbf{y}$ , the following matrix differentiation expression is used

$$\frac{\partial \mathbf{M}(\mathbf{y}) \mathbf{x}}{\partial \mathbf{y}} = \begin{bmatrix} \vdots \\ \mathbf{x}^T \frac{\partial \mathbf{m}_p^T}{\partial \mathbf{y}} \\ \vdots \end{bmatrix} \quad (\text{B.1})$$

331 where  $\mathbf{x}$  is a vector and  $\mathbf{m}_p$  denotes the  $p$ th row of the  $\mathbf{M}$  matrix.

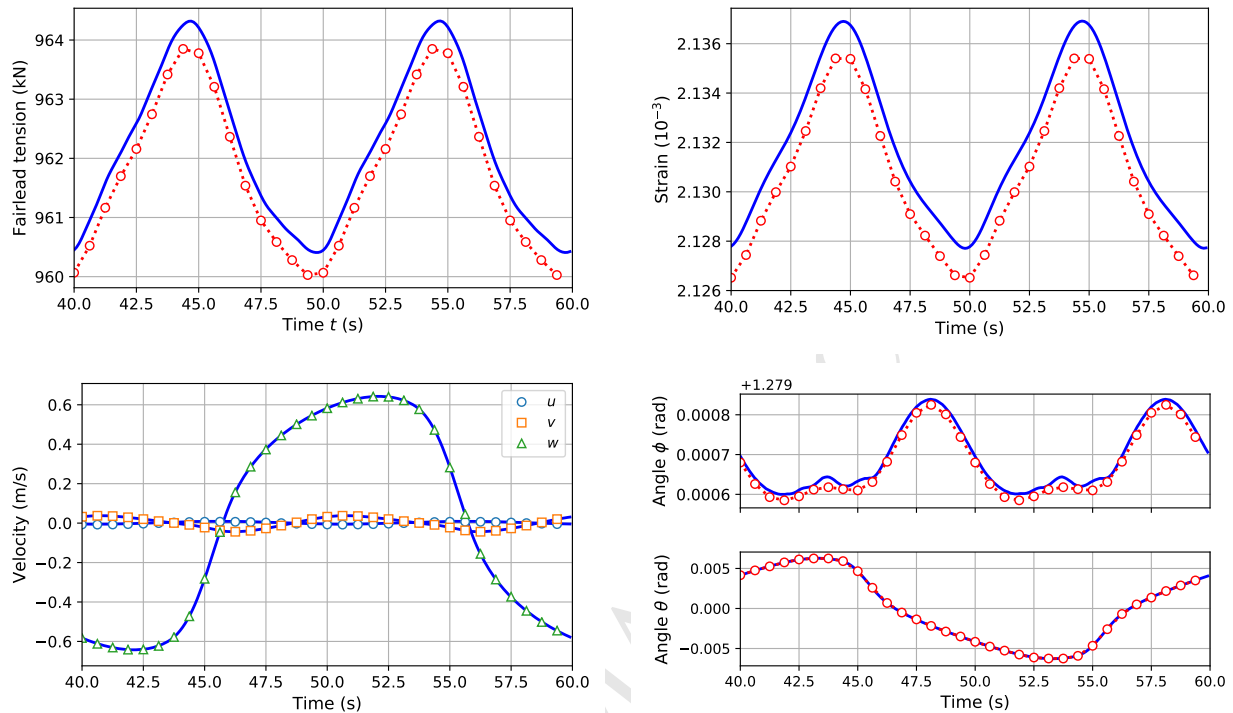


Figure 8: Comparison of the fairlead tension and nodal solution corresponding to the 25th node with  $s = 441.11$  m when the forced motion is in Z direction. Lines correspond to the time-domain analysis results and symbols indicate the multi-HB analysis results.

## References

- [1] S. Butterfield, W. Musial, J. Jonkman, P. Sclavounos, L. Wayman, Engineering challenges for floating offshore wind turbines, in: Proc. of the 2005 Copenhagen Offshore Wind Conference, The European Wind Energy Association, 2005, pp. 377–382.
- [2] D. Matha, M. Schlipf, R. Pereira, J. Jonkman, Challenges in simulation of aerodynamics, hydrodynamics, and mooring-line dynamics of floating offshore wind turbines, in: Proc. of the 21st Offshore and Polar Engineering Conference, International Society of Offshore and Polar Engineers, 2011.
- [3] B. W. Kim, H. G. Sung, J. H. Kim, S. Y. Hong, Comparison of linear spring and nonlinear fem methods in dynamic coupled analysis of floating structure and mooring system, *J. Fluids Struct.* 42 (2013) 205–227. doi:10.1016/j.jfluidstructs.2013.07.002.
- [4] M. Hall, B. Buckham, C. Crawford, Evaluating the importance of mooring line model fidelity in floating offshore wind turbine simulations, *Wind Energy* 17 (12) (2014) 1835–1853. doi:10.1002/we.1669.
- [5] J. Azcona, D. Palacio, X. Munduate, L. González, T. A. Nygaard, Impact of mooring lines dynamics on the fatigue and ultimate loads of three offshore floating wind turbines computed with IEC 61400-3 guideline, *Wind Energy* 20 (5) (2017) 797–813. doi:10.1002/we.2064.
- [6] J. E. Gutiérrez-Romero, J. García-Espinosa, B. Serván-Camas, B. Zamora-Parra, Non-linear dynamic analysis of the response of moored floating structures, *Mar. Struct.* 49 (2016) 116–137. doi:10.1016/j.marstruct.2016.05.002.
- [7] L. Chen, B. Basu, S. R. K. Nielsen, A coupled finite difference mooring dynamics model for floating offshore wind turbine analysis, *Ocean Eng.* 162 (2018) 304–315. doi:10.1016/j.oceaneng.2018.05.001.
- [8] B. Buckham, F. R. Driscoll, M. Nahon, Development of a finite element cable model for use in low-tension dynamics simulation, *J. Appl. Mech.* 71 (4) (2004) 476–485. doi:10.1115/1.1755691.
- [9] Y. H. Bae, Development of a dynamic mooring module FEAM for FAST v8, Report, Texas A&M University (2014).
- [10] E. Kreuzer, U. Wilke, Dynamics of mooring systems in ocean engineering, *Archive Appl. Mech.* 73 (3) (2003) 270–281. doi:10.1007/s00419-003-0288-3.
- [11] M. Hall, A. Goupee, Validation of a lumped-mass mooring line model with DeepCwind semisubmersible model test data, *Ocean Eng.* 104 (2015) 590–603. doi:10.1016/j.oceaneng.2015.05.035.
- [12] J. Azcona, X. Munduate, L. González, T. A. Nygaard, Experimental validation of a dynamic mooring lines code with tension and motion measurements of a submerged chain, *Ocean Eng.* 129 (2017) 415–427. doi:10.1016/j.oceaneng.2016.10.051.
- [13] A. A. Tjavaras, The dynamics of highly extensible cables, Thesis, Massachusetts Institute of Technology (1996).
- [14] A. A. Tjavaras, Q. Zhu, Y. Liu, M. S. Triantafyllou, D. K. P. Yue, The mechanics of highly-extensible cables, *J. Sound Vib.* 213 (4) (1998) 709–737. doi:10.1006/jsvi.1998.1526.

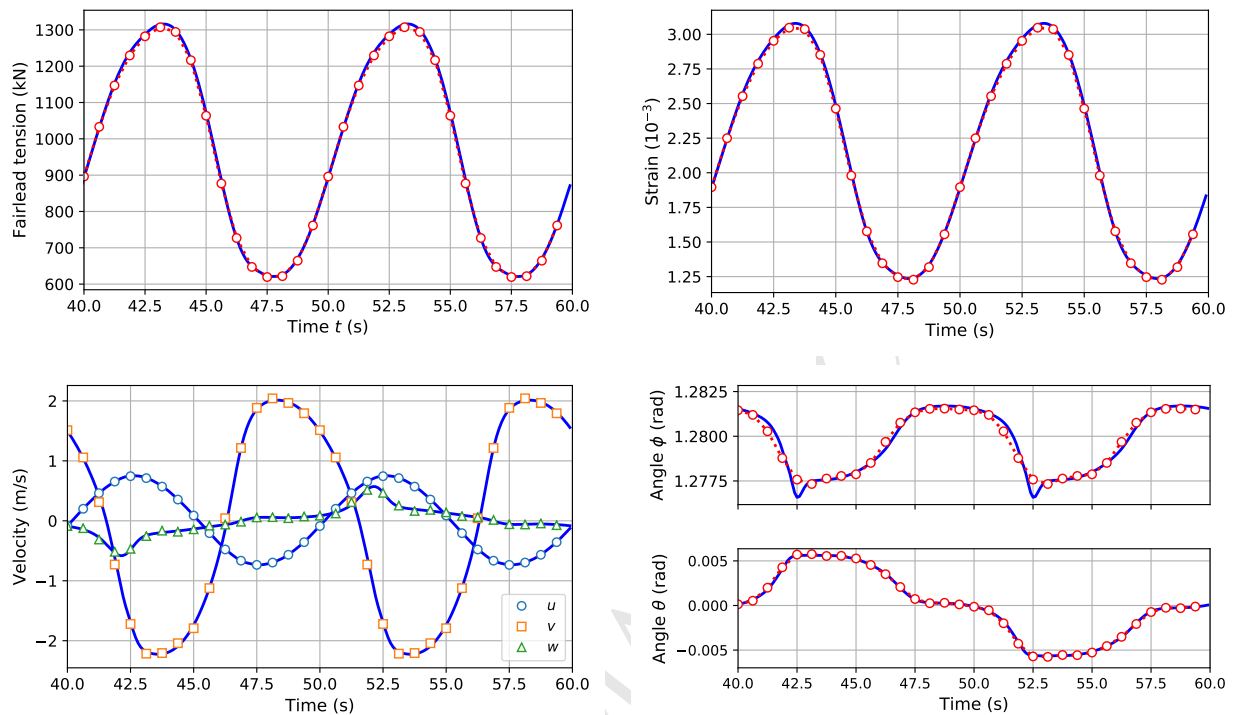


Figure 9: Comparison of the fairlead tension and nodal solution corresponding to the 25th node with  $s = 441.11$  m when the forced motion is in both  $Y$  and  $Z$  directions. Lines correspond to the time-domain analysis results and symbols indicate the multi-HB analysis results.

- 360 [15] J. I. Gobat, The dynamics of geometrically compliant mooring systems, Thesis, Massachusetts Institute of Technology (2000).
- 361 [16] J. I. Gobat, M. A. Grosenbaugh, Time-domain numerical simulation of ocean cable structures, *Ocean Eng.* 33 (10) (2006) 1373–1400.
- 362 [doi:10.1016/j.oceaneng.2005.07.012](https://doi.org/10.1016/j.oceaneng.2005.07.012).
- 363 [17] Y. Li, Q. Zhu, L. Liu, Y. Tang, Transient response of a spar-type floating offshore wind turbine with fractured mooring lines, *Renew. Energy*
- 364 122 (2018) 576–588. [doi:10.1016/j.renene.2018.01.067](https://doi.org/10.1016/j.renene.2018.01.067).
- 365 [18] J. Davidson, J. V. Ringwood, Mathematical modelling of mooring systems for wave energy converters – A Review, *Energies* 10 (5) (2017)
- 366 666. [doi:10.3390/en10050666](https://doi.org/10.3390/en10050666).
- 367 [19] J. B. Thomsen, F. Ferri, J. P. Kofoed, Screening of available tools for dynamic mooring analysis of wave energy converters, *Energies* 10 (7)
- 368 (2017) 853. [doi:10.3390/en10070853](https://doi.org/10.3390/en10070853).
- 369 [20] J. Palm, G. M. Paredes, C. Eskilsson, F. T. Pinto, L. Bergdahl, Simulation of mooring cable dynamics using a discontinuous Galerkin method,
- 370 in: *Proceedings of 5th International Conference on Computational Methods in Marine Engineering*, 2013, pp. 1–12.
- 371 [21] J. Palm, C. Eskilsson, L. Bergdahl, An  $hp$ -adaptive discontinuous galerkin method for modelling snap loads in mooring cables, *Ocean Eng.*
- 372 144 (2017) 266–276. [doi:10.1016/j.oceaneng.2017.08.041](https://doi.org/10.1016/j.oceaneng.2017.08.041).
- 373 [22] R. Antonutti, C. Peyrard, A. Incecik, D. Ingram, L. Johanning, Dynamic mooring simulation with code.aster with application to a floating
- 374 wind turbine, *Ocean Eng.* 151 (2018) 366–377. [doi:10.1016/j.oceaneng.2017.11.018](https://doi.org/10.1016/j.oceaneng.2017.11.018).
- 375 [23] F. S. Hover, Methods for positioning deeply-towed underwater cables, Thesis, Massachusetts Institute of Technology (1993).
- 376 [24] F. S. Hover, M. A. Grosenbaugh, M. S. Triantafyllou, Calculation of dynamic motions and tensions in towed underwater cables, *IEEE J.*
- 377 *Oceanic Eng.* 19 (3) (1994) 449–457. [doi:10.1109/48.312921](https://doi.org/10.1109/48.312921).
- 378 [25] A. Sarkar, R. Eatock Taylor, Dynamics of mooring cables in random seas, *J. Fluids Struct.* 16 (2) (2002) 193–212. [doi:10.1006/jflls.](https://doi.org/10.1006/jflls.2001.0415)
- 379 [2001.0415](https://doi.org/10.1006/jflls.2001.0415).
- 380 [26] Y. Liu, L. Bergdahl, Frequency-domain dynamic analysis of cables, *Eng. Struct.* 19 (6) (1997) 499–506. [doi:10.1016/S0141-0296\(96\)](https://doi.org/10.1016/S0141-0296(96)00091-0)
- 381 [00091-0](https://doi.org/10.1016/S0141-0296(96)00091-0).
- 382 [27] I. K. Chatjigeorgiou, Second-order nonlinear dynamics of catenary pipelines: A frequency domain approach, *Comput. Struct.* 123 (2013)
- 383 1–14. [doi:10.1016/j.compstruc.2013.04.006](https://doi.org/10.1016/j.compstruc.2013.04.006).
- 384 [28] N. M. Krylov, N. N. Bogoliubov, *Introduction to non-linear mechanics*, Vol. 11, Princeton University Press, 1943.
- 385 [29] W. J. Cunningham, *Introduction to non-linear analysis*, McGraw-Hill, 1958.
- 386 [30] M. Urabe, Galerkin's procedure for nonlinear periodic systems, *Archive Ration. Mech. Anal.* 20 (2) (1965) 120–152. [doi:10.1007/](https://doi.org/10.1007/BF00284614)
- 387 [BF00284614](https://doi.org/10.1007/BF00284614).
- 388 [31] F. H. Ling, X. X. Wu, Fast Galerkin method and its application to determine periodic solutions of non-linear oscillators, *Int. J. Non-Linear*

- 389 Mech. 22 (2) (1987) 89–98. doi:10.1016/0020-7462(87)90012-6.
- 390 [32] T. M. Cameron, J. H. Griffin, An alternating frequency/time domain method for calculating the steady-state response of nonlinear dynamic  
391 systems, *J. Appl. Mech.* 56 (1) (1989) 149–154. doi:10.1115/1.3176036.
- 392 [33] A. Cardona, T. Coune, A. Lerusse, M. Geradin, A multiharmonic method for non-linear vibration analysis, *Int. J. Numer. Methods Eng.* 37 (9)  
393 (1994) 1593–1608. doi:10.1002/nme.1620370911.
- 394 [34] J. P. Miralles, P. J. Jiménez Olivo, D. G. Peiró, G. V. Martín, J. M.-C. González, A fast Galerkin method to obtain the periodic solutions of a  
395 nonlinear oscillator, *Appl. Math. Comput.* 86 (23) (1997) 261–282. doi:10.1016/S0096-3003(96)00193-2.
- 396 [35] G. Kerschen, M. Peeters, J.-C. Golinval, A. F. Vakakis, Nonlinear normal modes, Part I: A useful framework for the structural dynamicist,  
397 *Mech. Syst. Signal Proc.* 23 (1) (2009) 170–194. doi:10.1016/j.ymsp.2008.04.002.
- 398 [36] M. Peeters, R. Viguí, G. Sérandour, G. Kerschen, J. C. Golinval, Nonlinear normal modes, Part II: Toward a practical computation using  
399 numerical continuation techniques, *Mech. Syst. Signal Proc.* 23 (1) (2009) 195–216. doi:10.1016/j.ymsp.2008.04.003.
- 400 [37] T. Detroux, L. Renson, G. Kerschen, The harmonic balance method for advanced analysis and design of nonlinear mechanical systems, in:  
401 *Nonlinear Dynamics, Volume 2*, Springer, 2014, pp. 19–34.
- 402 [38] L. Sun, L. Chen, Periodic responses of a taut cable attached with a friction damper computed using multi-harmonic balance method, in: *Proc.*  
403 *IABSE Guangzhou 2016, IABSE, Zurich, Switzerland*, 2016, pp. 464–471. doi:10.2749/222137816819258771.
- 404 [39] L. Chen, L. Sun, Steady-state analysis of cable with nonlinear damper via harmonic balance method for maximizing damping, *J. Struct. Eng.*  
405 143 (2) (2017) 04016172. doi:10.1061/(ASCE)ST.1943-541X.0001645.
- 406 [40] L. Sun, L. Chen, Residual mode correction in calibrating nonlinear damper for vibration control of flexible structures, *J. Sound Vib.* 406  
407 (2017) 197–207. doi:10.1016/j.jsv.2017.06.015.
- 408 [41] Y. Ni, G. Zheng, J. Ko, Nonlinear periodically forced vibration of stay cables, *Trans. ASME J. Vib. Acoust.* 126 (2) (2004) 245–252.  
409 doi:10.1115/1.1641800.
- 410 [42] M. Krack, L. Panning-von Scheidt, J. Wallaschek, A method for nonlinear modal analysis and synthesis: Application to harmonically forced  
411 and self-excited mechanical systems, *J. Sound Vib.* 332 (25) (2013) 6798–6814. doi:10.1016/j.jsv.2013.08.009.
- 412 [43] J. P. Breslin, Dynamic forces exerted by oscillating cables, *J. Hydronaut.* 8 (1) (1974) 19–31. doi:10.2514/3.62972.
- 413 [44] A. Bliet, Dynamic analysis of single span cables, Thesis, Massachusetts Institute of Technology (1984).
- 414 [45] J. R. Morison, J. W. Johnson, S. A. Schaaf, The force exerted by surface waves on piles, *J. Petroleum Technol.* 2 (05) (1950) 149–154.  
415 doi:10.2118/950149-G.
- 416 [46] W. H. Press, S. A. Teukolsky, W. T. Vetterling, B. P. Flannery, *Numerical Recipes in C: The art of scientific computing Second Edition*,  
417 Cambridge University Press, 2007.
- 418 [47] T. Detroux, L. Renson, L. Masset, G. Kerschen, The harmonic balance method for bifurcation analysis of large-scale nonlinear mechanical  
419 systems, *Comput. Methods Appl. Mech. Eng.* 296 (2015) 18–38. doi:10.1016/j.cma.2015.07.017.
- 420 [48] G. Guennebaud, B. Jacob, et al., *Eigen v3*, <http://eigen.tuxfamily.org> (2010).
- 421 [49] L. Chen, B. Basu, Fatigue load estimation of a spar-type floating offshore wind turbine considering wave-current interactions, *Int. J. Fatigue*  
422 (2018) (in press) doi:10.1016/j.ijfatigue.2018.06.002.
- 423 [50] J. Gobat, M. Grosenbaugh, Application of the generalized- $\alpha$  method to the time integration of the cable dynamics equations, *Computer*  
424 *methods in applied mechanics and engineering* 190 (37-38) (2001) 4817–4829. doi:10.1016/S0045-7825(00)00349-2.
- 425 [51] J. M. Jonkman, Definition of the floating system for phase IV of OC3, Report NREL/TP-500-47535, National Renewable Energy Laboratory  
426 (2010).
- 427 [52] J. M. Jonkman, D. Matha, Dynamics of offshore floating wind turbines—analysis of three concepts, *Wind Energy* 14 (4) (2011) 557–569.  
428 doi:10.1002/we.442.
- 429 [53] M. S. Triantafyllou, C. T. Howell, Dynamic response of cables under negative tension: an ill-posed problem, *J. Sound Vib.* 173 (4) (1994)  
430 433–447. doi:10.1006/jsvi.1994.1239.
- 431 [54] L. Chen, B. Basu, A numerical study on super-harmonic responses of mooring cables subjected to top end excitations, in: *International*  
432 *Symposium on the Dynamics and Aerodynamics of Cables (ISDAC2017)*, 2017, p. 291299.